

Evolution of a metal to insulator transition in $\text{Ca}_{2-x}\text{Na}_x\text{CuO}_2\text{Cl}_2$ as seen by angle-resolved photoemission

F. Ronning,^{1,*} T. Sasagawa,² Y. Kohsaka,² K. M. Shen,¹ A. Damascelli,^{1,†} C. Kim,^{1,‡} T. Yoshida,¹ N. P. Armitage,^{1,§} D. H. Lu,¹ D. L. Feng,^{1,†} L. L. Miller,³ H. Takagi,² and Z.-X. Shen¹

¹Department of Physics, Applied Physics and Stanford Synchrotron Radiation Laboratory, Stanford University, Stanford, California 94305

²Department of Advanced Materials Science, University of Tokyo, 7-3-1 Hongo, Bunkyo-ku, Tokyo 113-0033, Japan

³Department of Physics, Iowa State University, Ames, Iowa 50011

(Received 13 May 2002; published 2 April 2003)

We present angle resolved photoemission data on Na-doped $\text{Ca}_2\text{CuO}_2\text{Cl}_2$. We demonstrate that the chemical potential shifts upon doping the system across the insulator to metal transition. The resulting low-energy spectra reveal a gap structure which appears to deviate from the canonical $d_{x^2-y^2} \propto |\cos(k_x a) - \cos(k_y a)|$ form. To reconcile the measured gap structure with *d*-wave superconductivity one can understand the data in terms of two gaps, a very small one contributing to the nodal region and a very large one dominating the antinodal region. The latter is a result of the electronic structure observed in the undoped antiferromagnetic insulator. Furthermore, the low-energy electronic structure of the metallic sample contains a two component structure in the nodal direction, and a change in velocity of the dispersion in the nodal direction at roughly 50 meV. We discuss these results in connection with photoemission data on other cuprate systems.

DOI: 10.1103/PhysRevB.67.165101

PACS number(s): 74.25.Jb, 74.72.Jt, 79.60.Bm

I. INTRODUCTION

The close proximity of an antiferromagnetic Mott insulating phase suggests that this insulator may be the natural starting point for understanding the unusually high superconducting transition temperatures as well as the unconventional normal state properties¹ in the cuprates. The insulator to metal transition in strongly correlated materials is a well studied fundamental problem in solid state physics in its own right. Even by limiting ourselves to a one band Hubbard model, which may be an appropriate starting point for the half-filled cuprates,² there remain several ways one could imagine the electronic structure evolving upon doping (see Fig. 1). One scenario is the chemical potential shifting to the top of the valence band similar to the case of a band insulator.³ An alternative scenario is states being created inside the Mott gap upon doping.^{4,5} These are the two most commonly discussed pictures with regard to the cuprates.

Angle resolved photoemission spectroscopy (ARPES) studies of the $\text{La}_{2-x}\text{Sr}_x\text{CuO}_4$ (LSCO) system show that spectral weight is transferred to low-energy states, which lie inside the Mott gap, upon hole doping.^{4–7} In contrast, in the $\text{Bi}_2\text{Sr}_2\text{Ca}_{1-x}\text{Y}_x\text{Cu}_2\text{O}_{8+\delta}$ (Bi2212) and $\text{Nd}_{2-x}\text{Ce}_x\text{CuO}_4$ (NCCO) systems there is work which shows that the chemical potential shifts in addition to a transfer of spectral weight.^{8,9} A potential problem for the Bi2212 system is the difficulty to obtain deeply underdoped samples. The oxychlorides $\text{Sr}_2\text{CuO}_2\text{Cl}_2$ and $\text{Ca}_2\text{CuO}_2\text{Cl}_2$ are single layer cuprates that have provided the best photoemission data on the undoped insulating state to date. Thus the oxyhalides are ideal systems to study the metal to insulator transition with photoemission, as high quality single crystals, which cleave as easily as the Bi2212 system, can now be grown through the metal to insulator transition.

Recently, we have reported that the chemical potential

shifts upon doping the insulator $\text{Ca}_2\text{CuO}_2\text{Cl}_2$ (CCOC) with Na.¹⁰ Here we present the full body of evidence which supports arguments for such a shift of the chemical potential in the $\text{Ca}_{2-x}\text{Na}_x\text{CuO}_2\text{Cl}_2$ system. We examine the valence band and photon energy dependence of Na-doped CCOC and compare it with that found in the insulator. By making a detailed comparison of the low-energy spectra we unambiguously show that the high-energy pseudogap is in fact a result of the *d*-wave-like dispersion seen in the insulator, as had been suggested previously.^{11,12}

As we will show, residual effects from the insulator strongly distort the “band structure” in these deeply underdoped samples resulting in a gap structure along the LDA-predicted Fermi surface that strongly deviates from the canonical $d_{x^2-y^2}$ form. In order to reconcile this result with *d*-wave superconductivity, we conclude that the measured gap structure is a consequence of probing two different regimes. One regime is concerned with a small unresolved gap

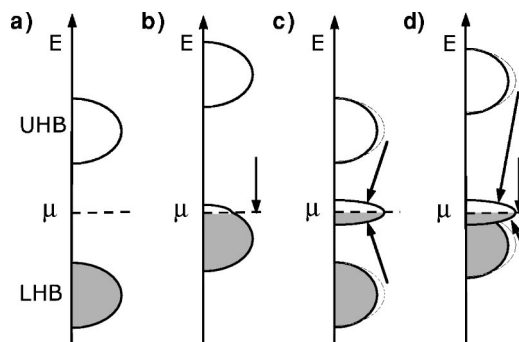


FIG. 1. Schematic doping evolution of an insulator. (a) Upper (UHB) and lower (LHB) Hubbard bands for a Mott Insulator. (b) Result of doping holes into a band insulator. (c) Result of creating states inside the gap with doping. (d) A scenario combining the ideas of (b) and (c).

along a hole pocket about $(\pi/2, \pi/2)$. The second regime is in the vicinity of $(\pi, 0)$ where a large gap, which we identify as the pseudogap, is identified with the undoped insulator. This picture is consistent with the observed chemical potential shift.

The evolution of the electronic structure, however, is not solely a simple shift of the chemical potential since the spectral lineshape also evolves with doping. We further investigate here the two component structure found in the nodal direction of $\text{Ca}_{2-x}\text{Na}_x\text{CuO}_2\text{Cl}_2$.¹⁰ We show that this structure is not directly related to T_c , and from a momentum distribution curve (MDC) analysis we find a “kink” in the dispersion which has the same energy as the “dip” which divides the two components in the energy distribution curves (EDC’s). The observation of a kink near 50 meV in this system supports the observed universality of this type of behavior in the cuprates.¹³ Finally, we discuss the similarities and differences between photoemission results from other cuprates and Na-doped CCOC.

II. EXPERIMENTAL

Na-doped CCOC single crystals were grown by a flux method under high pressure, by using a cubic anvil type pressure apparatus.¹⁴ A powder mixture of $\text{Ca}_2\text{CuO}_2\text{Cl}_2$, NaCl , NaClO_4 , and CuO (1:0.2:0.2:0.1 molar ratio), sealed in a gold tube, was heated to 1250°C and then slowly cooled to 1050°C under high pressure. Uniform samples at various Na concentrations x were achieved by using different pressures during the synthesis. 4 and 5 GPa gave a Na concentration of 10 and 12%, respectively. Crystals with a maximum dimension of $1.5 \times 1.5 \times 0.1 \text{ mm}^3$ were obtained. The Na content was estimated by comparing the c -axis lattice constant with powdered ceramic samples of known content.¹⁵ Magnetization measurements of T_c gave results consistent with the assigned doping concentrations. The Na concentrations used in this study were $x=0.10$ ($T_c=13\text{ K}$) and $x=0.12$ ($T_c=22\text{ K}$). Since superconductivity does not occur until $x \sim 0.08$ in the Na-doped CCOC system,^{14,15} we consider our samples to lie in the heavily underdoped regime. As a reference, the optimal T_c in powder samples has been found to be 28 K.¹⁵ ARPES measurements were performed on beamline 5–4 of SSRL. The samples were easily cleaved *in situ* and measured at the indicated temperatures in the figure captions. The angular resolution was 0.29° , while the energy resolution was always $\leq 30 \text{ meV}$. When examining the detailed low energy excitations (i.e., after Fig. 7) the energy resolution was improved to $\leq 15 \text{ meV}$.

III. DATA AND RESULTS

A. Valence band

We begin with the valence band spectra of Na-doped CCOC in Fig. 2, which illustrates a peculiarity of this system. Namely, from 8 to 13 eV binding energy there exists several pronounced features which rapidly vanish with time. The spectra from the cleave where these features were most prominent is shown in the top panel. Features are visible at 9, 10, and 12 eV which are not observed in the parent com-

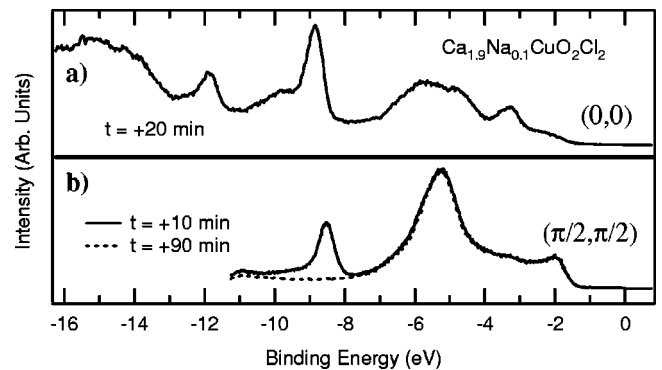


FIG. 2. (a) ARPES data reveals three features, at roughly 9, 10, and 12 eV, in Na-doped CCOC not present in the pure sample. The time elapsed between the initial cleave and the time the spectra were recorded is indicated. (b) illustrates, with a different cleave, how the features vanish within 90 min of the initial cleave. The photon energy was 25.5 eV and the temperature was 20 K. The Fermi cutoff on the low energy spectral weight is too small to be visible in this intensity scale.

pound, CCOC. Figure 2(b) reveals that within 90 min following the initial cleave, the additional features from 8 to 11 eV have vanished. The feature at 12 eV also vanishes (not shown). For binding energies less than 7 eV no change in the spectra was observed over these time scales where particularly close attention was paid to the near E_F features, less than 1 eV binding energy. The photon energy was adjusted to ensure the high binding energy features were not derived from a contribution of second order light from the monochromator. Comparing the spectra in panels (a) and (b) suggests a dispersive nature of the additional peaks not seen in the insulating compound. However, it was also observed that these features shift to lower binding energy as they age. We tentatively assign the origin of these features from 8 to 13 eV binding energy to flux inclusions, such as NaCl and NaClO_4 which are used in excess during the synthesis,¹⁶ subsequently the surface of these flux inclusions are passivated by the photon flux following the cleave. Despite the uncertain nature of these high-energy features, the fact that the low binding energy region of the spectra have no variation over the short time scale in which the high-energy features vanish, gives us confidence that our low-energy results on the Na-doped CCOC crystals are intrinsic.

Figure 3 compares the valence band spectra along the nodal direction for $x=0$ and $x=0.1$. The data on the insulator are consistent with previous reports on a similar material ($\text{Sr}_2\text{CuO}_2\text{Cl}_2$),^{17,18} and the data for the Na-doped $\text{Ca}_2\text{CuO}_2\text{Cl}_2$ were reproduced on multiple cleaves. The position of the valence band in the insulator with respect to the chemical potential can vary as much as 1 eV which is believed to be a result of pinning the chemical potential at different impurity levels that exist for the different cleaved surfaces. It is important to note that the valence band data of the insulator shown in Fig. 3 and 4 are at the minimum possible binding energy, since if they are shifted further towards the chemical potential, spectral weight from the tail of the valence band peaks would be pushed above the chemical

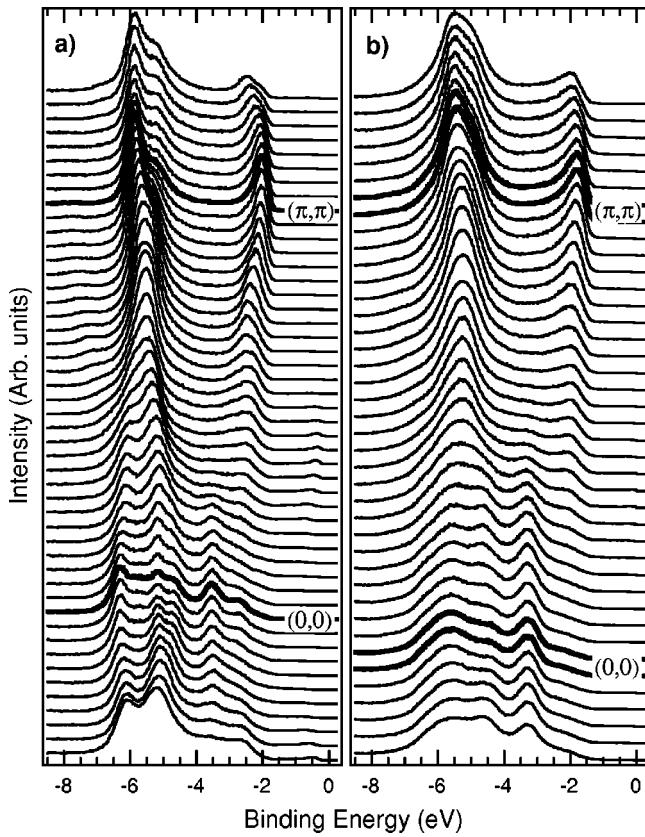


FIG. 3. Valence band spectra along the nodal direction for (a) $\text{Ca}_2\text{CuO}_2\text{Cl}_2$ and (b) 10% Na-doped CCOC. $E_\gamma=25.5$ eV, $T=200$ and 20 K for $x=0$ and $x=0.1$, respectively.

potential falsely indicative of a metallic nature. The low-energy excitations within 1 eV of the chemical potential, which the remainder of this paper will focus on, are barely visible on this broad scale. Generally, the two data sets are quite similar, although differing relative intensities for a few of the bands about $(0,0)$ can be seen. The other difference is that the insulator data are sharper than those of the metal. Perhaps this is an indication that the surface of Na-doped $\text{Ca}_2\text{CuO}_2\text{Cl}_2$ is not as well ordered as the pure sample grown under atmospheric conditions. Figure 4(a) plots the second derivative of the above spectra, which can be used to more clearly identify the dispersion of various features. This method agrees with the dispersion extracted by the peak positions of the various bands in the insulator and the metal as shown in Fig. 4(b). The resolved bands appear to have shifted to lower binding energy with doping by roughly 300 meV, as would be expected if this were a simple band material. One apparent exception exists from the band at 5.6 eV binding energy in the metallic sample near $(0,0)$ in Fig. 4(b). However, due to the broadness of the features in the metal, it is likely that this band is a superposition of several peaks, resulting in this apparent discrepancy. Note that in the insulator several bands are resolved in this same region. Thus, the overall picture from the valence band data is highly suggestive of a chemical potential shift with doping. The most convincing demonstration for this is at (π,π) where the peaks for both concentrations are most clearly resolved.

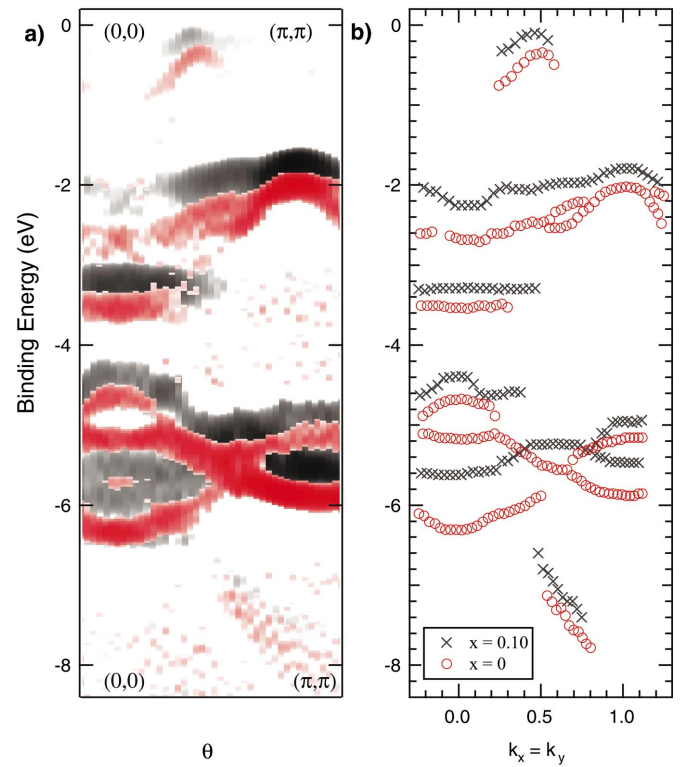


FIG. 4. (Color) Valence band comparison of $\text{Ca}_2\text{CuO}_2\text{Cl}_2$ and 10% Na-doped CCOC. (a) A second derivative plot of the EDC's presented in Fig. 3 retaining only points with negative curvature and (b) maps the dispersion of the various features as seen by eye. The measurement conditions are identical except for the temperature of the insulator which is raised to avoid electrostatic charging during the photoemission process. $E_\gamma=25.5$ eV, $T=200$ and 20 K for $x=0$ and $x=0.1$, respectively. The data are consistent with a shift of the chemical potential with doping as discussed in the text.

Here, the peak positions indicate that the insulator is shifted to higher energy by at least 300 meV relative to the metal. The specific value will depend on which insulating data set is used, since the chemical potential in the insulator can vary substantially as mentioned above. We again emphasize that the current binding energy of the insulator could not be found at smaller binding energies without spectral weight being shifted unrealistically above the chemical potential. Thus, neither charging of the insulator nor the variability of the chemical potential in the insulator can be responsible for the observed shift upon doping.

B. Near E_F comparison

To further support this idea, Fig. 5 presents spectra near E_F along the entire $(0,0)$ to $(\pi,0)$ and $(0,0)$ to (π,π) lines, where all the spectra from this insulating data set have been shifted by 750 meV so that the centroid of the feature at $(\pi/2, \pi/2)$ is at the chemical potential. The value of 750 meV is specific to this particular data set, but is 300 meV more than allowed by the uncertainty in the position of the chemical potential. Along $(0,0)$ to $(\pi,0)$ the spectra are remarkably similar. In many instances fine details of the line shape match extremely well. For example, a second broad component in

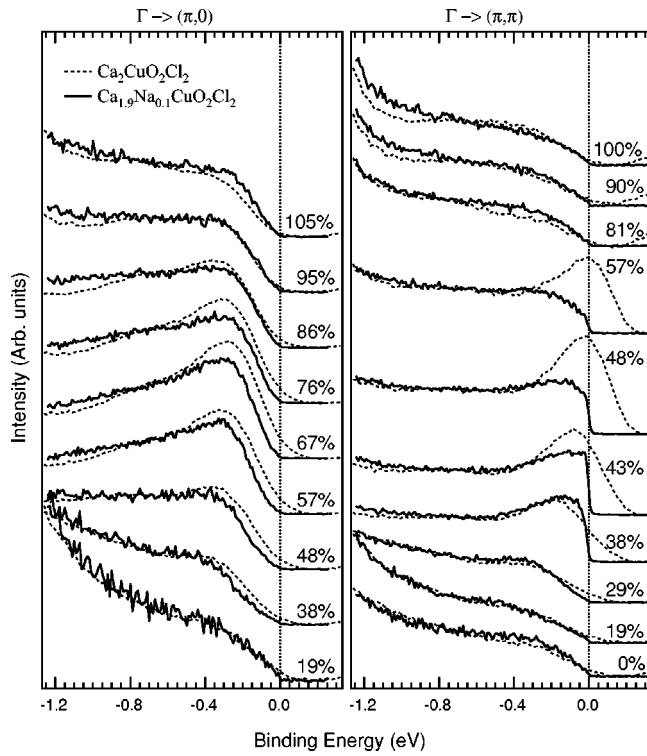


FIG. 5. EDC's of $\text{Ca}_2\text{CuO}_2\text{Cl}_2$ (dashed line) (from Ref. 12) are shifted by a constant in energy and compared with EDC's of 10% Na-doped CCOC (solid line). The overlap is extremely good with the exception of the features near $(\pi/2, \pi/2)$. The data are normalized at high binding energy for comparison. The slight rise in spectral weight above E_F observed in some EDC's of CCOC is due to the presence of a core level excited by second order light. This is not present in the metallic sample where the second order light contribution is heavily suppressed by the use of a normal incidence monochromator as opposed to the grazing incidence monochromator used for the insulating data. $E_\gamma = 25.5$ eV, $T = 100$ and 20 K for $x=0$ and $x=0.1$, respectively.

the electronic structure can be observed at roughly 600 meV higher binding energy from the first feature creating a heavily asymmetric line shape.^{19,20} This indicates that upon doping the chemical potential simply drops to intersect the top of the valence band similar to the case of an ordinary band material. This would naturally explain the large high energy pseudogap seen at $(\pi, 0)$ as a remnant property of the insulator as first suggested by Laughlin.^{11,12}

Along $(0,0)$ to (π, π) the situation is less clear. As the feature moves towards lower binding energy a sharp Fermi cutoff appears in the metallic samples, as anticipated by the large peak at the Fermi level from the energetically shifted spectra of the insulating sample. However, the match between the spectra becomes increasingly worse as $(\pi/2, \pi/2)$ is approached. Perhaps this simply indicates that a Fermi crossing has occurred before $(\pi/2, \pi/2)$, and thus the weight at $(\pi/2, \pi/2)$ is suppressed relative to the insulator or that some spectral weight transfer in addition to the shift of the chemical potential has occurred. To see if the suppression was due to matrix element effects we also changed the polarization to maximize the nodal direction cross section, but it

remained weaker. This suppression possibly indicates that increased scattering which could effectively smear out the k resolution, and would have the greatest effect where the dispersion is the steepest [near $(\pi/2, \pi/2)$], has occurred. However, this would require a nontrivial small angle scattering mechanism, which does not simply produce an angle independent background. Also, the cleavability of the Na-doped compounds is the same as the parent insulator, and laser reflections from the sample indicate flat surfaces, which argue against angle averaging as the cause for the observed suppression of weight. Typically, highly angle dependent valence band spectra as shown in Fig. 3 are indicative of a good surface, although the Na-doped valence band features are somewhat broader than in the case of the insulator. Pothuizen *et al.*¹⁸ noted that in SCOC the line shape of the 2 eV binding energy peak at (π, π) is identical to the line shape of the Zhang-Rice singlet at $(\pi/2, \pi/2)$. Given such a correlation a broadened low-energy spectral line shape at $(\pi/2, \pi/2)$ in Na-doped CCOC is perhaps expected when the valence band at 2 eV has been broadened, as observed here (see Fig. 3). This suggests that the small differences between the doped system and the half filled insulator may indeed result from a difference in sample surface quality.

Considering that the features of hole doped CCOC track the dispersion of the features in the half filled insulator, one might wonder exactly how similar are the electronic states for the two doping levels. A good way to test this is by analyzing the photoemission matrix elements. Under the dipole approximation the photoemission intensity can be written as $I \propto |\langle \Psi_f | A \cdot p | \Psi_i \rangle|^2$ where $\Psi_{i,f}$ are the initial and final state wave functions, and $A \cdot p$ is the perturbing Hamiltonian.²¹ Practically, this means that the cross section of the photoemission process will depend on the photon energy and experimental geometry as well as the wave functions themselves. Thus, if two wave functions are to be considered as the same, then they should have the same dependence on the experimental conditions. We have found that CCOC experiences a fairly dramatic change in the modulation of intensity along the nodal direction when changing the photon energy from 16.5 to 17.5 eV. In Fig. 6, we compare the EDC's along the nodal direction of a 10% Na-doped CCOC sample and an undoped CCOC sample using 16.5 and 17.5 eV photons. We notice that the change in the modulating intensity on going from $E_\gamma = 16.5$ to 17.5 eV is similar for both samples. Namely, for 16.5 eV photons there is much more intensity at $(\pi/2, \pi/2)$ and higher k values, which vanishes on going to 17.5 eV photons. Even the existence of the second feature at 600 meV higher binding energy from the lowest-energy feature can be seen in both samples along the nodal direction. These results show that the gross features of the wave function of the electronic states within 2 eV of the chemical potential discussed thus far are remarkably similar. The peculiar photon energy dependence shown in Fig. 6 will be discussed separately with a much larger body of data.²² Along with the fairly rigid shift in dispersion of the low-energy states and the valence band, the line shape comparison and photon energy dependence show conclusively that the chemical potential indeed shifts upon doping the half filled insulator $\text{Ca}_2\text{CuO}_2\text{Cl}_2$ with Na.

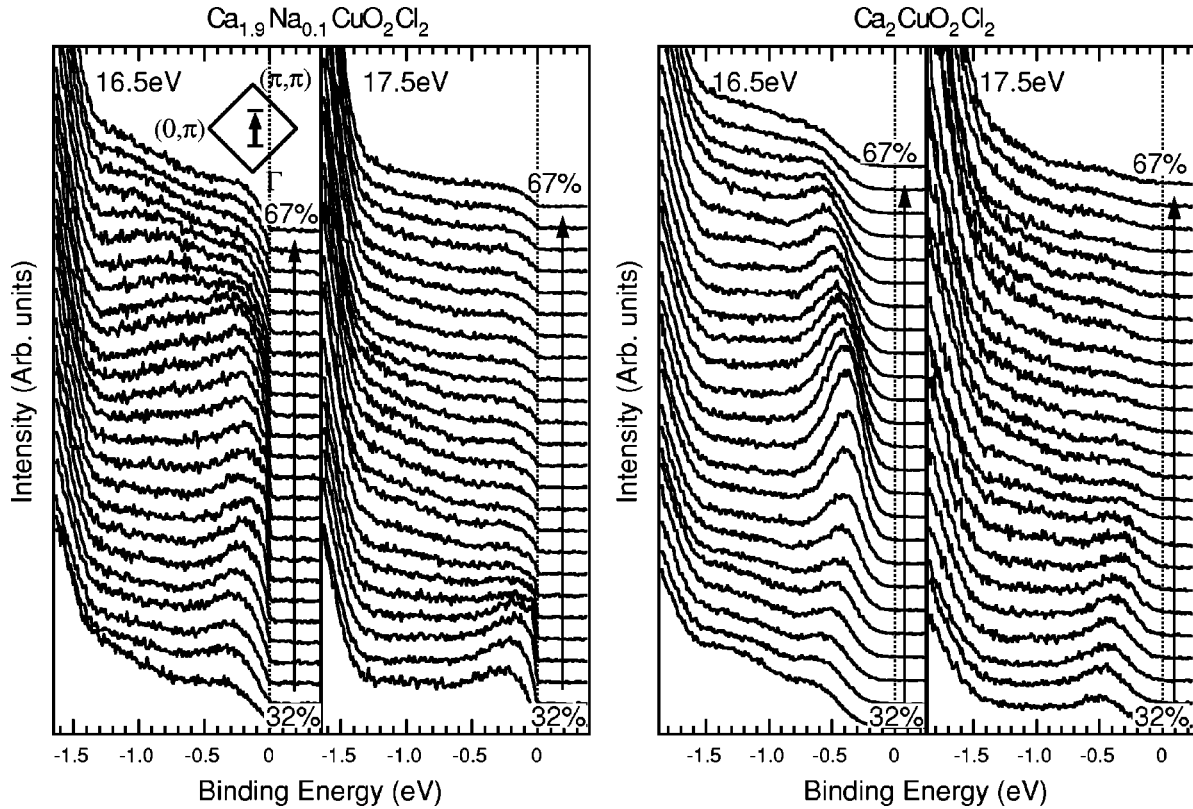


FIG. 6. Photon energy dependence along the nodal direction for $\text{Ca}_{2-x}\text{Na}_x\text{CuO}_2\text{Cl}_2$ for $x=0.1$ and $x=0$. For each doping, the same k range is shown, while the photon energy is indicated in each panel. $T=20$ and 293 K for $x=0.1$ and 0.0, respectively. Notice, that the modulation of intensity varies with photon energy in a similar fashion for both dopings.

C. Metallic nature of Na-doped $\text{Ca}_2\text{CuO}_2\text{Cl}_2$

A naive expectation of a simple chemical potential shift upon doping is the creation of a small hole pocket centered at $(\pi/2, \pi/2)$. However this contrasts with the majority of ARPES results from the optimal and overdoped regime which find a large Fermi surface centered about (π, π) as predicted by band theory.²³ We shall thus take a closer look at the near E_F electronic structure to see if the simple picture of a chemical potential shift as illustrated in Fig. 1(b) is correct. In other words, is the electronic structure unchanged with the exception of the position of the chemical potential? Figure 7 presents a sampling of the EDC's at selected k points. The cuts shown in (a) through (d) are taken parallel to the nodal direction. For several of the cuts close to the nodal direction a broad feature starts at high binding energy and approaches the Fermi energy with increasing k , where a sharp Fermi cutoff of the spectra is indicative of a Fermi surface crossing. We will return to the presence of a peak-dip-hump-like structure near the nodal Fermi crossing later. The Fermi crossings, which have been determined by the spectra with the minimum leading edge midpoint (the binding energy where the spectral intensity is half of the intensity at the peak position), have been highlighted in the figure. We note that while a minimum value of the leading edge midpoint identifies the spectra which corresponds to k_F , the value itself will be pushed back to higher binding energy if this portion of the Fermi surface is gapped. As the cuts approach $(\pi, 0)$ the spectral features become less pronounced

and it quickly becomes impossible to identify a Fermi crossing as one can no longer clearly identify a peak position to meaningfully extract a leading edge. This is best illustrated in panel (e) where spectra along the ostensible Fermi surface predicted by band theory are presented. Near the node, there is a clear Fermi cutoff at E_F , but this feature disappears quickly as one approaches the antinodal region.

One can also visualize the data with an intensity map at E_F , obtained by integrating each EDC by a ± 4 meV window about E_F . The highest intensity contour, shown in Fig. 8(a), forms what appears as a small arc.²⁴ The open circles indicate where a clear Fermi crossing can be observed as in the cuts shown in Figs. 7(a)–7(c). Note this ends as the Fermi surface crosses the antiferromagnetic zone boundary. By assuming that the Fermi surface cannot abruptly end in the middle of the Brillouin zone, one is left with two possibilities. Either the Fermi surface still lies along the one predicted by band theory and has been heavily gapped as one approaches $(\pi, 0)$ or the Fermi surface is a small hole pocket centered on or near $(\pi/2, \pi/2)$. We investigate these two possibilities below.

Let us first attempt to push the assumption that the large LDA-like Fermi surface holds for this heavily underdoped sample. We separate the large Fermi surface into two regions, as illustrated in Fig. 8(b). In region I the broad spectral function has a sharp Fermi cutoff, which clearly defines k_F , while in region II one must extrapolate the Fermi surface from the Fermi crossings found in region I assuming a large

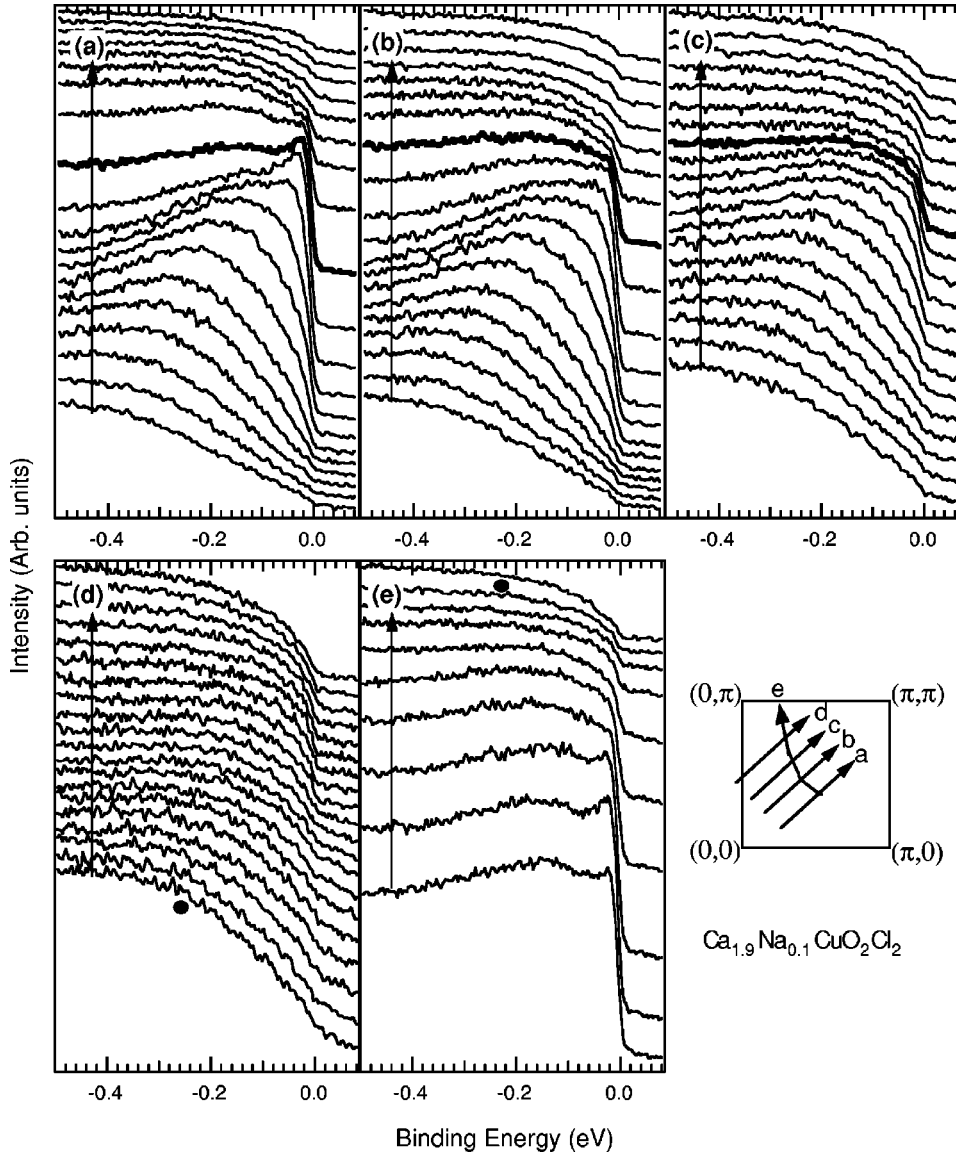


FIG. 7. Selected EDC's of Na-doped $\text{Ca}_2\text{CuO}_2\text{Cl}_2$ taken at the k points shown by solid lines in the diagrams. The lines in the Brillouin zone indicate all the k points where spectra were taken. The bold spectra in (a) through (c) indicate k_F . No spectra are highlighted in (d) as no Fermi crossing is observed. Spectra along the Fermi surface predicted by band theory are shown in (e). The dots in (d) and (e) indicate a high energy feature as discussed in the text. $E_\gamma = \text{He}$, $I\alpha = 21.2 \text{ eV}$, $T = 22 \text{ K}$

Fermi surface that does not terminate in the middle of the Brillouin zone. This is shown by the solid dots in Fig. 8. Note that in the region near $(\pi, 0)$, variations in the precise shape of the Fermi surface will not affect the following analysis as the spectra have little variation which is apparent from the EDC's in Fig. 7(d).

Figure 9 plots the leading edge midpoint for spectra along the large Fermi surface just discussed relative to the value at $\phi = 45^\circ$ (the nodal position for a pure $d_{x^2-y^2}$ functional form). In this way one can determine the gap structure along the Fermi surface. The open symbols indicate the leading edge midpoint for the Fermi crossing spectra found in region I. However, in region II the lack of a clear leading edge midpoint prevented us from identifying a Fermi crossing in the first place. Hence, we need an alternative method to describe the dispersion. Near $(\pi, 0)$ an energy scale (albeit a broad one) still exists in the spectra as indicated by a dot in Figs. 7(d) and 7(e). Thus we can blindly normalize the maximum of the spectra below 300 meV to 1, and extract a lead-

ing edge midpoint via this simplified approach. This is what is shown by the filled symbols in Fig. 9. For a simple spectral function this procedure would give the correct gap value. In our case, one can see that close to the node this procedure roughly matches our more careful analysis, but it also allows us to extend our gap analysis beyond the regime where a clear Fermi crossing has been identified, albeit in a crude way. The solid black line is the expectation for the canonical d -wave functional form. As mentioned above, in the optimal and overdoped Bi2212 samples a simple spectral function and a large Fermi surface is observed, and the d -wave functional form well describes the experimental gap structure.²⁵ However, in the heavily underdoped regime studied here, there is a strong deviation from the d -wave functional form. In order to reconcile this gap structure with d -wave superconductivity²⁶ our assumption of a large Fermi surface centered at (π, π) must break down. In this case, Fig. 9 is not physically significant as it maps the energy along two physically different regions as defined in Fig. 8(b), each with

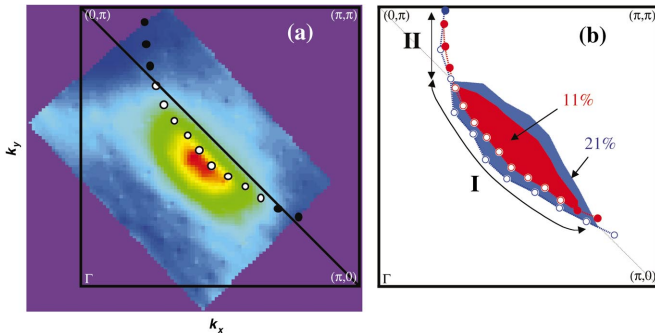


FIG. 8. (Color) (a) E_F map obtained by integrating the $x = 0.10$ spectra by ± 4 meV about E_F . The open dots indicate the Fermi crossing, while the solid dots extrapolate the Fermi surface to the Brillouin zone edge as would be expected in band theory. (b) An illustration indicating the area of the resulting Fermi surface pocket obtained by symmetrizing the observed Fermi crossings about the antiferromagnetic zone boundary (dashed gray line). By counting the number of electrons in the enclosed area a doping level is found which is indicated in the figure. Red reproduces the points in (a) for $x = 0.10$, while blue are results from a sample with $x = 0.12$. The data naturally fall into two regimes: I(II) distinguishes the region along the underlying LDA Fermi surface where a clear Fermi crossing does (does not) occur.

its own gap structure. In other words, by assuming a d -wave gap structure we have shown that only a fraction of the spectra used for Fig. 9 actually lie on the Fermi surface.

Region I does indeed represent a portion of the Fermi surface about $(\pi/2, \pi/2)$ which may contain a very small gap, while region II does not contain a Fermi crossing, and

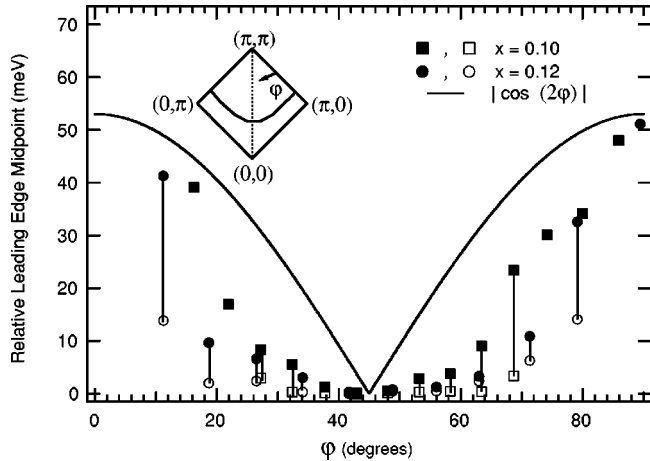


FIG. 9. The leading edge midpoint of the spectra along the Fermi surface illustrated in Fig. 8 relative to the value at the d -wave nodal position. The open symbols are the result when a clear Fermi cutoff can be identified, while the solid symbols are obtained by normalizing the maximum of the low energy spectra to 1, as discussed in the text. The solid line is a plot of $\cos(2\phi)$, the d -wave functional form. The large discrepancy from the canonical d -wave functional form when attempting to describe the data in terms of a band-theory-like Fermi surface centered at (π, π) suggests that it is better to understand the data in terms of two regimes, labeled I and II in Fig. 8.

the resulting large gap identifies a larger energy scale. We have just ruled out the possibility that the Fermi surface in this sample is a large hole pocket centered at (π, π) . If we maintain that the Fermi surface can not abruptly end in the middle of the Brillouin zone we must conclude that the Fermi surface forms a small hole pocket, as naively expected from the observed chemical potential shift. The question then becomes, how does such a Fermi surface develop a gap consistent with d -wave superconductivity. Given the experimental resolution we cannot comment on whether or not the flat region in Fig. 9 would itself fit a $|\cos(k_x a) - \cos(k_y a)|$ functional form, which is the simplest expectation for d -wave pairing, although models exist with small hole pockets and d -wave pairing for which this is not the case.²⁸ We note that for a superconductor with a transition temperature of 13 K, the maximum of the gap from BCS theory is expected to be less than 2 meV at the antinode and even smaller along the observed arc, which is too small for our experimental resolution and is not the objective of this study. Perhaps this gap could be measured with an improved spectrometer.

By symmetrizing the hole pocket about the antiferromagnetic zone boundary one finds an area of 5.7%, which implies a doping level of 11.4% due to the electron spin. This is in rough agreement with the hole doping of 10% determined by comparing T_c and lattice constants with results on powdered samples.¹⁵ Again we note that the hole pocket is also not necessarily symmetric about the antiferromagnetic zone boundary,²⁸ which could substantially modify these values. The idea of a small hole pocket about $(\pi/2, \pi/2)$ in Na-doped CCOC is also consistent with the observations of shadow bands²⁷ at higher binding energy.¹⁰ Presumably, the coherence factors responsible for the shadow band are very weak making it difficult to distinguish a second Fermi crossing from the background at E_F . We stress that while our findings are quite consistent with the small Fermi pocket picture, we did not see the shadow Fermi surface at zero energy even though we do observe a shadow band at higher energies.

Meanwhile, the observation of a chemical potential shift in this material from the insulating state and the photon energy dependence of the lineshape emphasize that the features near $(\pi, 0)$ (region II) in the Na-doped $\text{Ca}_2\text{CuO}_2\text{Cl}_2$ sample are a direct result of the magnetism which dominates the antiferromagnetic insulator. To illustrate that the energy scale near $(\pi, 0)$ is the same as that of the insulator, recall Fig. 5 where the spectra of the insulator matches that of the Na-doped sample at $(\pi, 0)$.

We have also repeated the above gap structure analysis on a sample with $x = 0.12$ ($T_c = 22$ K), and some of the results are presented in blue in Fig. 8 and as circles in Fig. 9. The data reproduce the above analysis with a few small quantitative differences. The Fermi arc increases in size (shown in Fig. 8b), consistent with an increase in doping, while the binding energy near $(\pi, 0)$ reduces slightly which demonstrates that this energy scale is decreasing with increasing doping. This is also expected as we have identified this energy scale with the magnetism of the insulator whose strength should diminish together with the antiferromagnetic correlations as holes are added to the system. This has also

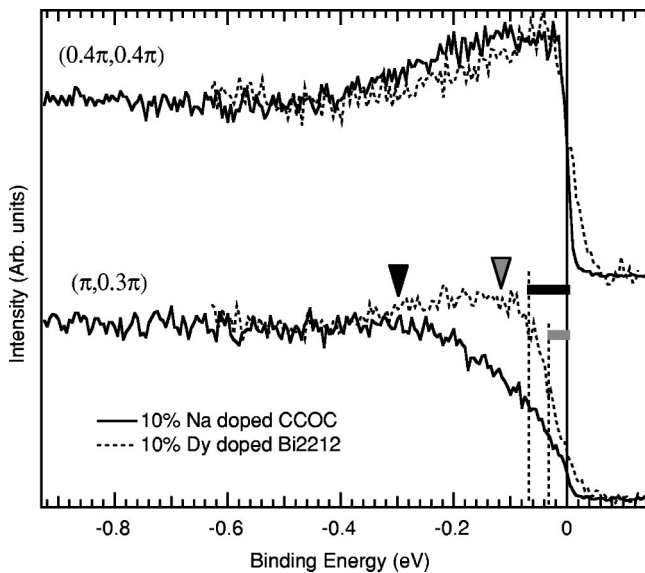


FIG. 10. Comparison of EDC's at selected k points of 10% Dy-doped Bi2212 (taken from Ref. 31) and 10% Na-doped CCOC. The Na-doped CCOC system suggests a much larger pseudogap than in Bi2212, both for the low energy pseudogap (thick bars) and the high-energy pseudogap (triangles).

been observed in previous studies on the high-energy pseudogap.²⁹ We should note that the hidden message of describing the Fermi surface in the underdoped regime as a small pocket about $(\pi/2, \pi/2)$ is that the system must at some point transform upon doping to the large Fermi surface centered about (π, π) observed in the overdoped regime. In measuring the volume of the pocket for the $x=0.12$ sample we find the doping level to be 21%. The fact that this analysis begins to show a deviation from a doping level of x perhaps begins to identify a transition to a state where the doping level should be described as $1-x$ [the expected volume of the large Fermi surface centered at (π, π)].³⁰

In comparison with other cuprates, the lack of a Fermi cutoff in the EDC's would normally be identified as an extremely large pseudogap. In an attempt to quantify this suppression of weight, we compare 10% Na-doped CCOC to 10% Dy-doped Bi2212 (Ref. 31) in Fig. 10. 10% Dy-doped Bi2212 is underdoped with a T_c of 65 K giving it a $T_c/\max(T_c)$ of 0.72, while 10% Na-doped CCOC has a ratio of 0.46. A comparison with 17.5% Dy-doped Bi2212 (not shown) with a $T_c/\max(T_c)$ ratio of 0.28 yielded a similar comparison. One clearly observes the loss of spectral weight at the Fermi energy for the Fermi momentum of $(\pi, 0.3\pi)$ when compared to the respective Fermi crossings along the nodal direction near $(0.4\pi, 0.4\pi)$. There are two common methods for characterizing the pseudogap with ARPES. The first is by the shift of the leading edge midpoint of a spectra to higher binding energy relative to the chemical potential as indicated by the dashed lines. This is typically referred to as the low-energy pseudogap. For Dy-doped Bi2212 this is reasonably well defined, and gives a value of 30 meV. For the Na-doped CCOC sample, we find a value of roughly 50 meV at $(\pi, 0.3\pi)$. However, as previously noted, the lack of a

Fermi cutoff near $(\pi, 0)$ implies that the low-energy pseudogap is not well defined in the Na-doped CCOC spectra. As a result, we are inclined to characterize the pseudogap by what is known as the high-energy pseudogap which identifies a larger energy scale in the spectra about $(\pi, 0)$, and is sometimes referred to as a “hump.”²⁹ Here, we find a high-energy pseudogap of roughly 300 meV for Na-doped CCOC, compared with 120 meV for Dy-doped Bi2212 as indicated by the triangles in Fig. 10. Independent of the method chosen, the pseudogap for Na-doped CCOC appears significantly larger than that of Bi2212 at a comparable doping level.

The high-energy pseudogap seen in Bi2212 was first conjectured by Laughlin to be a result of the d -wave-like modulation of the dispersion of the insulating oxyhalides.^{11,12} From the observed shift of the chemical potential it is clear that the high-energy pseudogap indeed directly results from the dispersion seen in the parent compound, although it appears that the energy scales of the high-energy pseudogap have a small system dependent variation. The implication for such a large pseudogap relative to the Bi2212 system at comparable doping should be investigated, and the bilayer effect in Bi2212 will need to be taken into consideration. If the condensation energy for superconductivity is acquired by the gapping of low-energy states near $(\pi, 0)$, then this would result in superconductivity being less favorable as evidenced by the smaller optimal T_c (28 and 90 K for Na-doped CCOC and Bi2212, respectively).

D. Nodal peak-dip-hump structure

A two component structure can be seen in the low-energy spectra of Na-doped CCOC at the Fermi crossing in the nodal direction. This was shown in Fig. 7(e), where we plotted EDC's along the Fermi arc and then towards $(\pi, 0)$ as indicated in the cartoon inset. The reason for the difference in clarity of this structure between cleaves is unknown, but is likely due to a variation of inhomogeneities and experimental conditions which make it impossible to resolve the two components that appear as one in the $(0.43\pi, 0.43\pi)$ spectra of Fig. 5. Note that in general, the presence of sharp low-energy features is a tribute to a high sample quality. The loss of the two component structure as one approaches $(\pi, 0)$ is indicative of the observed large pseudogap, which precludes the identification of any similar structure in the low-energy excitations near $(\pi, 0)$.

The observation of a two component structure in these superconducting samples begs the question of how it may be related to superconductivity. Figure 11 presents temperature dependence of this feature from 20 K ($\approx T_c$) up to 120 K. It is clear that the peak-dip-hump-like structure is observed up to 75 K, and is finally smeared out at 120 K. By cycling the temperature back down to 20 K, we ensure that the broadening at high temperatures is not an aging effect. Since even optimally doped polycrystalline samples have only a maximum T_c of 28 K, it is clear that the two component structure observed here does not turn on near T_c . This is in contrast with the more familiar two component structure in ARPES on the Bi2212 system which has now also been seen in

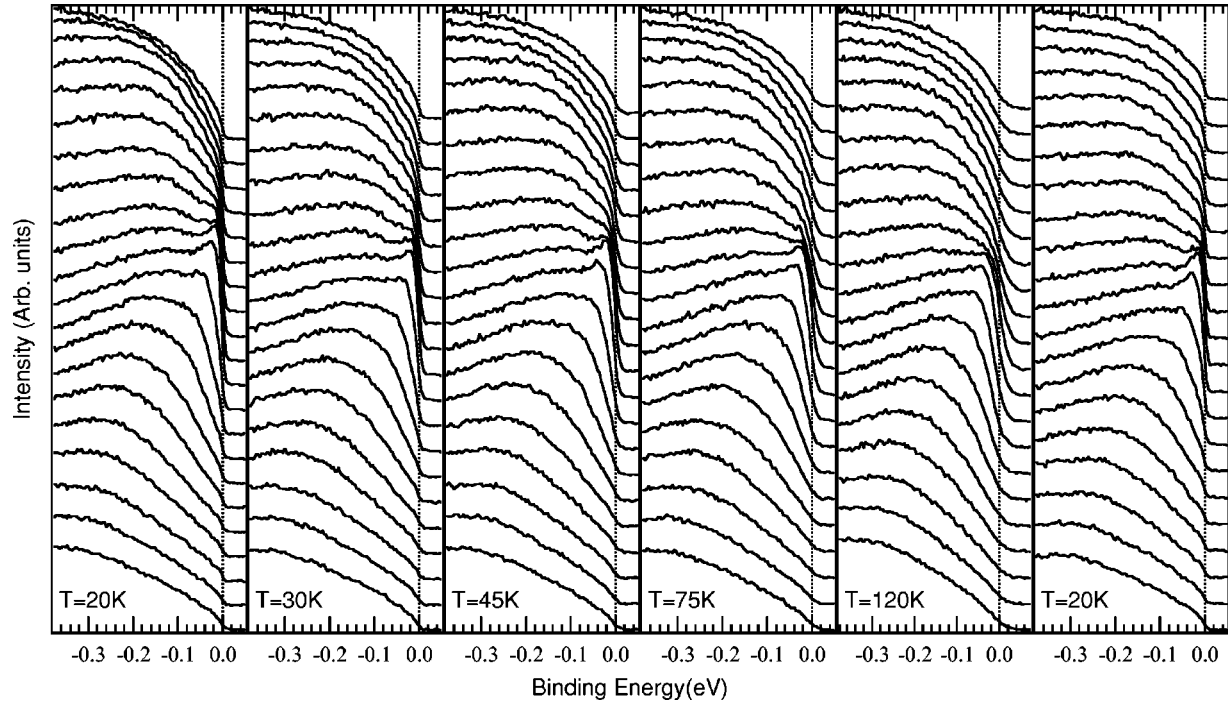


FIG. 11. (a) Temperature dependence of 12% Na-doped CCOC along the nodal direction. A two component structure is observed at k_F well above T_c . $E_\gamma = 16.5$ eV.

YBCO Ref. 32 and Bi2223,³³ and does turn on with T_c .^{34,35} It is important to note that, aside from the different temperature dependence, the two component structure observed in Na-doped CCOC occurs along the nodal direction as opposed to the $(\pi, 0)$ region as in the other cases. Furthermore, we note that CCOC is a single layer material and thus the peak-dip-hump seen here can not be a consequence of bilayer splitting as has been conjectured for the peak-dip-hump structure observed in Bi2212.³⁶

In order to gain some insight into the origin of this structure Fig. 12 presents a MDC analysis along the nodal direction of a $x=0.10$ sample. The dashed curves are the single Lorentzian fits to selected MDC's. Similar procedure in other cuprates has been used to extract self-energies from the fit parameters.^{13,37,38} Here the fits serve as a method for parametrizing the observed dispersion. Figures 12(b) and 12(c) plot the peak positions and widths as a function of the binding energy of the corresponding MDC's. A change of slope in the dispersion of the peak positions is seen near 55 meV. This value is attained from the intersection of two linear fits ranging from 0 to 30 meV and 100 to 200 meV. We shall refer to this feature as a “kink.” A similar kink in other cuprate systems has received significant attention in recent ARPES literature.^{13,38–40} Certainly, the similarity of the kink energy position to the dip energy position seen in the EDC's suggests that these two results are related. The MDC width also displays an accelerated decrease in width as indicated by the dotted lines in Fig. 12(c).

What is the possible origin of a two component structure in the EDC near k_F along the nodal direction? Pure macroscopic phase separation of metallic and undoped insulating domains can be ruled out, since the feature seen in the insu-

lator would not have shifted to the chemical potential in this case. One possibility is that a sharp, coherentlike peak is growing with doping, while the incoherent features at half filling slowly vanish. This idea is captured in the recent phase string calculations done by Muthukumar, Weng, and Sheng.⁴¹ In this sense, the two components would hint at a balance between the antiferromagnetic insulator and the drive for the system to become metallic. An alternative scenario is that the peak-dip-hump structure is the result of coupling to a collective mode. This could also naturally explain the presence of the kink. Although still a debated interpretation, Lanzara *et al.* propose that the universally observed kink is due to electron-phonon coupling.¹³ In this regard, it is interesting to note that the phonon breathing mode is expected to be roughly 10 meV less for CCOC on the basis of its a -axis lattice constant than in the case of insulating Bi2212 or LSCO as determined by optics,⁴² while the kink energy position determined by ARPES is less by roughly the same amount.

Distinguishing between these two scenarios will be difficult. A problem with the first picture would be that the kink would have to be explained as an artifact of the MDC analysis due to the multiple electronic features which are not individually resolved. This is not appealing considering the apparent universality of the kink feature among cuprates,¹³ and one would then favor a coupling to a collective mode. However, it is surprising that the kink is seen in both LSCO where the states were created inside the gap, and in Na-doped CCOC where the states appear to originate from the effective lower Hubbard band which has now been shifted to the chemical potential. This suggests that a third possibility, combining both ideas, may also be considered for the doping

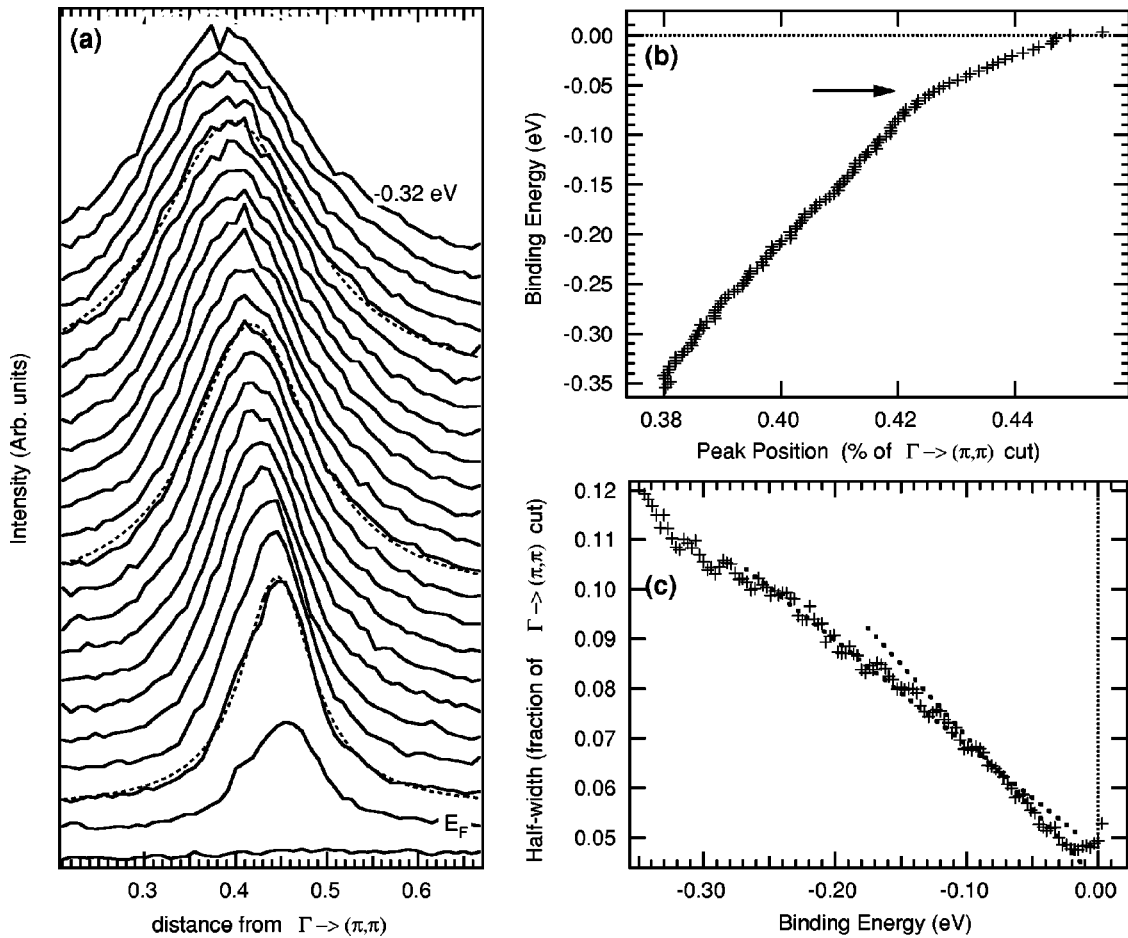


FIG. 12. (a) Sample MDC's of $\text{Ca}_{1.9}\text{Na}_{0.1}\text{CuO}_2\text{Cl}_2$ from the nodal direction taken with He $I\alpha$ radiation. Single Lorentzian fits to selected MDC's are overlayed with a dotted line. Respectively, (b) and (c) give the peak positions and widths (half width at half maximum) from the MDC analysis. The arrow in (b) indicates the kink energy, as discussed in the text.

evolution. Namely, that the chemical potential has shifted upon doping, the precise location would be system dependent, while states are created at E_F which then couple to some collective excitations creating the universally observed kink [see Fig. 1(d)]. If this is the case, the $\text{Ca}_{2-x}\text{Na}_x\text{CuO}_2\text{Cl}_2$ and $\text{La}_{2-x}\text{Sr}_x\text{CuO}_4$ system would no longer appear so different. Unfortunately, the present data can not distinguish between these three possibilities, and we must leave this as an opportunity for future experiments with more available doping levels to investigate.

IV. CONCLUSIONS AND DISCUSSION

The data from the valence band, near E_F spectra, and photon energy dependence in the $\text{Ca}_{2-x}\text{Na}_x\text{CuO}_2\text{Cl}_2$ system provide convincing evidence that the chemical potential shifts to the top of the valence band upon doping the insulator $\text{Ca}_2\text{CuO}_2\text{Cl}_2$. Surprisingly, these results appear to present a different evolution across the metal to insulator transition than in LSCO where the chemical potential is pinned and states are created inside the gap upon doping.⁵

With the comparison of CCOC we have shown that the high-energy pseudogap is indeed a remnant property of the

insulator.¹¹ Meanwhile, by examining the low lying excitations we found that an attempt to use a large Fermi surface centered at (π, π) results in a gap structure which deviates from the canonical d -wave functional form. Instead a small Fermi pocket about $(\pi/2, \pi/2)$ as naively expected from a rigid chemical potential shift is a better description of heavily underdoped $\text{Ca}_{2-x}\text{Na}_x\text{CuO}_2\text{Cl}_2$. This is the case when we insist that the Fermi surface can not terminate at a point in the middle of the Brillouin zone. A Fermi surface arc could also explain the data if this were allowable in a non-Fermi-liquid picture. We anticipate this region to also possess a gap structure which could differentiate between competing models in the underdoped regime. Finally, a two component structure is also observed in the EDC's along the nodal direction. This appears to be related to a kink seen in the MDC derived dispersion, which is now a universally observed feature of the cuprates.¹³

The presence of features seen in the insulator within the low energy spectra of the Na-doped superconductor suggests a strong interplay between antiferromagnetism and superconductivity in the underdoped regime. One way to think of these results is to start from the overdoped regime where superconductivity is the first instability encountered. Upon

further underdoping, magnetism begins to play a role which opens a large pseudogap, and suppresses superconductivity. Alternatively, one can start with the insulator, which forms a small pocket as carriers are introduced into the system. Superconductivity then creates a new instability that opens a small gap along the Fermi surface, which we are unable to detect given our resolution. We look forward to future experiments which will clarify $\text{Ca}_{2-x}\text{Na}_x\text{CuO}_2\text{Cl}_2$'s evolution to the more "conventional" behavior of the overdoped regime, and its relation to the other cuprate superconductors.

ACKNOWLEDGMENTS

F.R. would like to thank M.B. Walker and N. Schwanger for generously providing assistance to facilitate completion of this work, as well as A.-M.S. Tremblay and S.C. Zhang for helpful discussions. This research was carried out at the Stanford Synchrotron Radiation Laboratory which is operated by the D.O.E. Office of Basic Energy Science, Division of Chemical Sciences. The Office's Division of Material Science provided funding for this research. The Stanford work is also supported by NSF Grant No. DMR-0071897.

*Present Address: Dept. of Physics, University of Toronto, 60 St. George St, Toronto, ON, M5S 1A7, Canada.

[†]Present Address: Dept. of Physics and Astronomy, University of British Columbia, Vancouver, Canada.

[‡]Present Address: Dept. of Physics, Yonsei University, Seoul, Korea.

[§]Present Address: Dept. of Physics and Astronomy, UCLA, Los Angeles, CA.

¹T. Timusk and B. Statt, Rep. Prog. Phys. **62**, 61 (1999).

²P.W. Anderson, Science **235**, 1196 (1987).

³M.B.J. Meinders, H. Eskes, and G.A. Sawatzky, Phys. Rev. B **48**, 3916 (1993).

⁴J.W. Allen, C.G. Olson, M.B. Maple, J.-S. Kang, L.Z. Liu, J.-H. Park, R.O. Anderson, W.P. Ellis, J.T. Markert, Y. Dalichaouch, and R. Liu, Phys. Rev. Lett. **64**, 595 (1990).

⁵A. Ino, C. Kim, M. Nakamura, T. Yoshida, T. Mizokawa, Z.-X. Shen, A. Fujimori, T. Kakeshita, H. Eisaki, and S. Uchida, Phys. Rev. B **62**, 4137 (2000).

⁶H. Romberg, M. Alexander, N. Nücker, P. Adelmann, and J. Fink, Phys. Rev. B **42**, 8768 (1990).

⁷C.T. Chen, F. Sette, Y. Ma, M.S. Hybertsen, E.B. Stechel, W.M.C. Foulkes, M. Schulter, S-W. Cheong, A.S. Cooper, L.W. Rupp, Jr., B. Batlogg, Y.L. Soo, Z.H. Ming, A. Krol, and Y.H. Kao, Phys. Rev. Lett. **66**, 104 (1991).

⁸M.A. van Veenendaal, G.A. Sawatzky, and W.A. Groen, Phys. Rev. B **49**, 1407 (1994).

⁹N. Harima, J. Matsuno, A. Fujimori, Y. Onose, Y. Taguchi, and Y. Tokura, Phys. Rev. B **64**, 220507(R) (2001).

¹⁰Y. Kohsaka, T. Sasagawa, F. Ronning, T. Yoshida, C. Kim, T. Hanaguri, M. Azuma, M. Takano, Z.-X. Shen, and H. Takagi, cond-mat/0209339; J. Phys. Soc. Jpn. **72** (5) (to be published in 2003).

¹¹R.B. Laughlin, Phys. Rev. Lett. **79**, 1726 (1997).

¹²F. Ronning, C. Kim, D.L. Feng, D.S. Marshall, A.G. Loeser, L.L. Miller, J.N. Eckstein, I. Bozovic, and Z.-X. Shen, Science **282**, 2067 (1998).

¹³A. Lanzara, P.V. Bogdanov, X.J. Zhou, S.A. Kellar, D.L. Feng, E.D. Lu, T. Yoshida, H. Eisaki, A. Fujimori, K. Kishio, J.-i. Shimoyama, T. Noda, S. Uchida, Z. Hussain, and Z.-X. Shen, Nature (London) **412**, 510 (2001).

¹⁴Y. Kohsaka, M. Azuma, I. Yamada, T. Sasagawa, T. Hanaguri, M. Takano, and H. Takagi, J. Am. Chem. Soc. **124**, 12275 (2002).

¹⁵Z. Hiroi, N. Kobayashi, and M. Takano, Nature (London) **371**, 139 (1994); Z. Hiroi, N. Kobayashi, and M. Takano, Physica C **266**, 191 (1996).

¹⁶B.C. Beard, Surf. Sci. Spectra **2**, 91 (1994); *ibid.* **2**, 97 (1994).

¹⁷C. Dürr, S. Legner, R. Hayn, S.V. Borisenko, Z. Hu, A. Theresiak,

M. Knupfer, M.S. Golden, J. Fink, F. Ronning, Z.-X. Shen, H. Eisaki, S. Uchida, C. Janowitz, R. Muller, R.L. Johnson, K. Rossnagel, L. Kipp, and G. Reichardt, Phys. Rev. B **63**, 014505 (2000).

¹⁸J.J.M. Pothuizen, R. Eder, N.T. Hien, M. Matoba, A.A. Menovsky, and G.A. Sawatzky, Phys. Rev. Lett. **78**, 717 (1997).

¹⁹C. Kim, P.J. White, Z.-X. Shen, T. Tohyama, Y. Shibata, S. Maekawa, B.O. Wells, Y.J. Kim, R.J. Birgeneau, and M.A. Kastner, Phys. Rev. Lett. **80**, 4245 (1998).

²⁰F. Ronning, Ph.D. thesis, Stanford University, 2001.

²¹S. Hüfner, *Photoelectron Spectroscopy: Principles and Application* (Springer-Verlag, New York, 1995).

²²K.M. Shen, F. Ronning, T. Sasagawa, Y. Kohsaka, H. Takagi, and Z.-X. Shen (unpublished).

²³A. Damascelli, Z. Hussain, and Z.-X. Shen, cond-mat/0208504; Rev. Mod. Phys. **75** (2) (to be published in April 2003); D.W. Lynch and C.G. Olson, *Photoemission Studies of High-Temperature Superconductors* (Cambridge University Press, Cambridge, 1999); Z.-X. Shen and D.S. Dessau, Phys. Rep. **253**, 1 (1995), and references therein.

²⁴M.R. Norman, H. Ding, M. Randeria, J.C. Campuzano, T. Yokoya, T. Takeuchi, T. Takahashi, T. Mochiku, K. Kadokami, P. Guptasarma, and D.G. Hinks, Nature (London) **392**, 157 (1998).

²⁵Z.-X. Shen, D.S. Dessau, B.O. Wells, D.M. King, W.E. Spicer, A.J. Arko, D. Marshall, L.W. Lombardo, A. Kapitulnik, P. Dickinson, S. Doniach, J. DiCarlo, T. Loeser, and C.H. Park, Phys. Rev. Lett. **70**, 1553 (1993).

²⁶The Na-doped CCOC samples have been measured at a temperature above T_c . However, ARPES work on underdoped Bi2212 find a large Fermi surface with an identical gap structure above and below T_c consistent with the d -wave functional form. See A.G. Loeser *et al.*, Science **273**, 325 (1996); H. Ding *et al.*, Nature (London) **382**, 51 (1996).

²⁷A.P. Kampf and J.R. Schrieffer, Phys. Rev. B **42**, 7967 (1990).

²⁸See for example X.-G. Wen and P.A. Lee, Phys. Rev. Lett. **80**, 2193 (1998).

²⁹P.J. White, Z.-X. Shen, C. Kim, J.M. Harris, A.G. Loeser, P. Fournier, and A. Kapitulnik, Phys. Rev. B **54**, R15 669 (1996).

³⁰S. Uchida, T. Ido, H. Takagi, T. Arima, Y. Tokura, and S. Tajima, Phys. Rev. B **43**, 7942 (1991).

³¹D.S. Marshall, D.S. Dessau, A.G. Loeser, C-H. Park, A.Y. Matsuurra, J.N. Eckstein, I. Bozovic, P. Fournier, A. Kapitulnik, W.E. Spicer, and Z.-X. Shen, Phys. Rev. Lett. **76**, 4841 (1996).

³²D.H. Lu, D.L. Feng, N.P. Armitage, K.M. Shen, A. Damascelli, C. Kim, F. Ronning, Z.-X. Shen, D.A. Bonn, R. Liang, W.N. Hardy, A.I. Rykov, and S. Tajima, Phys. Rev. Lett. **86**, 4370 (2001).

³³D.L. Feng, A. Damascelli, K.M. Shen, N. Motoyama, D.H. Lu, H.

- Eisaki, K. Shimizu, J.-i. Shimoyama, K. Kishio, N. Kaneko, M. Greven, G.D. Gu, X.J. Zhou, C. Kim, F. Ronning, N.P. Armitage, and Z.-X. Shen, Phys. Rev. Lett. **88**, 107001 (2002).
- ³⁴D.L. Feng, D.H. Lu, K.M. Shen, C. Kim, H. Eisaki, A. Damascelli, R. Yoshizaki, J.-i. Shimoyama, K. Kiskio, G.D. Gu, S. Oh, A. Andrus, J. O'Donnell, J.N. Eckstein, and Z.-X. Shen, Science **289**, 277 (2000).
- ³⁵H. Ding, J.R. Engelbrecht, Z. Wang, J.C. Campuzano, S.-C. Wang, H.-B. Yang, R. Rogan, T. Takahashi, K. Kadokawa, and D.G. Hinks, Phys. Rev. Lett. **87**, 227001 (2001).
- ³⁶A.A. Kordyuk, S.V. Borisenko, T.K. Kim, K.A. Nenkov, M. Knupfer, J. Fink, M.S. Golden, H. Berger, and R. Follath, Phys. Rev. Lett. **89**, 077003 (2002).
- ³⁷T. Valla, A.V. Fedorov, P.D. Johnson, Q. Li, G.D. Gu, and N. Koshizuka, Phys. Rev. Lett. **85**, 828 (2000).
- ³⁸P.V. Bogdanov, A. Lanzara, S.A. Kellar, X.J. Zhou, E.D. Lu, W.J. Zheng, G. Gu, J.-I. Shimoyama, K. Kishio, H. Ikeda, R. Yoshizaki, Z. Hussain, and Z.-X. Shen, Phys. Rev. Lett. **85**, 2581 (2000).
- ³⁹A. Kaminski, M. Randeria, J.C. Campuzano, M.R. Norman, H. Fretwell, J. Mesot, T. Sato, T. Takahashi, and K. Kadokawa, Phys. Rev. Lett. **86**, 1070 (2001).
- ⁴⁰P.D. Johnson, T. Valla, A.V. Fedorov, Z. Yusof, B.O. Wells, Q. Li, A.R. Moodenbaugh, G.D. Gu, N. Koshizuka, C. Kendziora, Sha Jian, and D.G. Hinks, Phys. Rev. Lett. **87**, 177007 (2001).
- ⁴¹V.N. Muthukumar, Z.Y. Weng, and D.N. Sheng, Phys. Rev. B **65**, 214522 (2002).
- ⁴²S. Tajima, T. Ido, S. Ishibashi, T. Itoh, H. Eisaki, Y. Mizuo, T. Arima, H. Takagi, and S. Uchida, Phys. Rev. B **43**, 10 496 (1991).